Appl. Phys. A 85, 277–286 (2006)
DOI: 10.1007/s00339-006-3722-x

Applied Physics A
Materials Science & Processing

J.S. KULKARNI[1]
O. KAZAKOVA[2]
J.D. HOLMES[1,✉]

Dilute magnetic semiconductor nanowires

[1] Materials Section and Supercritical Fluid Centre, Department of Chemistry, University College Cork, Cork, Ireland
[2] National Physical Laboratory, Teddington, UK

Received: 28 April 2006/Accepted: 31 July 2006
Published online: 29 September 2006 • **© Springer-Verlag 2006**

ABSTRACT Semiconductor materials form the basis of modern electronics, communication, data storage and computing technologies. One of today's challenges for the development of future technologies is the realization of devices that control not only the electron charge, as in present electronics, but also its spin, setting the basis for future spintronics. Spintronics represents the concept of the synergetic and multifunctional use of charge and spin dynamics of electrons, aiming to go beyond the traditional dichotomy of semiconductor electronics and magnetic storage technology. The most direct method to induce spin-polarized electrons into a semiconductor is by introducing appropriate transition-metal or rare-earth dopants producing a dilute magnetic semiconductor (DMS). At the same time the seamless integration of future spintronic devices into nanodevices would require the fabrication of one-dimensional DMS nanostructures in well-defined architectures. In this review we focus on recent advances in the synthesis of DMS nanowires as well discussing the structural, optical and magnetic properties of these materials.

PACS 75.75.+a; 81.07.Vb; 68.65.La

1 Introduction

Semiconductor materials are an integral part of modern electronics, communication, data storage and computing technologies. Two conditions form the basis of these technologies: precise control and manipulation of electric charge transport in semiconductors, and the ability to use these materials for efficient generation and detection of light. One of today's challenges for the development of future technologies is the realization of devices that control not only the electron charge, as in present electronics, but also its spin, setting the basis for future spintronics. Spintronics represents the concept of the synergetic and multifunctional use of charge and spin dynamics of electrons, aiming to go beyond the traditional dichotomy of semiconductor electronics and magnetic storage technology. Control over the electronic spin largely increases the information that the electron carries and, therefore, opens up novel technological horizons. The electron spin is far less disturbed by the semiconductor environment than its other physical properties, such as the velocity and spatial position of the carriers. The spin-coherence time, i.e. the time in which the spin loses its phase information, is therefore relatively long. This is particularly important for future devices that will be based on the quantum properties of matter. The most direct method to induce spin-polarized electrons into a semiconductor is by introducing appropriate transition-metal or rare-earth dopants (such as Mn, Fe or Ni) at a level of a few per cent, producing a dilute magnetic semiconductor (DMS) [1–4]. Extensive research has been carried out in order to create DMS materials with well-established room-temperature ferromagnetism. Encouragingly, a Curie temperature, T_c, above room temperature was first theoretically predicted in GaN and ZnO hosts doped with Mn by the hole-mediated exchange interaction model [5] and later observed experimentally in thin-film samples [6, 7]. However, despite such promising results, most DMS materials are still struggling to reliably achieve the desired high T_c required for use in practical applications. During the last few years high-temperature ferromagnetism has been observed in a variety of wide band gap semiconductors, including GaN, AlN, GaP, SiC, ZnO, etc., doped with the whole range of transition metals, such as Cr, Mn, Fe, Co and Ni [8–12]. Conversely, room-temperature ferromagnetism in narrow band gap group IV semiconductors like $Ge_{1-x}Mn_x$ was not expected. In particular, a T_c value of 80 K for $Ge_{0.95}Mn_{0.05}$ thin films has been calculated by Dietl et al. [5] using a Zener model. Recently, effective pair exchange interactions in $Ge_{1-x}Mn_x$ have also been studied by ab initio computational methods by Kudrnovsky et al. [13]. Those authors showed that T_c is dependent on the Mn concentration, being up to 175 K at a Mn concentration of 3.5%. Experimentally, it has been demonstrated that in epitaxially grown $Ge_{1-x}Mn_x$ films T_c increases linearly with Mn concentration from 25 K to 116 K [14], whereas bulk $Ge_{0.94}Mn_{0.06}$ single crystals have been reported to have a T_c of 285 K [15]. Recently, it has been shown that co-doping $Ge_{1-x}Mn_x$ with an additional transition metal such as iron or cobalt causes significant increases in both magnetic moment and T_c [16, 17]. Moreover, complementary doping using dopants from different groups of elements (e.g. Mn and Co in the Ge host) compensates the effects of lattice strain caused by

✉ Fax: +353-(0)-21-4274097, E-mail: j.holmes@ucc.ie

the doping species and may eventually lead to realization of highly doped magnetoelectronic materials.

The recent interest in chemically grown semiconductor nanowires arises from their versatility, which translates into a wide range of potential applications. Many essential prototype devices have already been provided, such as elementary logic circuits [18], resonant tunnelling diodes [19], light-emitting diodes [20], lasers [21] and chemical sensors [22]. For example, field-effect transistors based on 1D semiconductor heterostructures were recently demonstrated [23]. Such structures are fully compatible with conventional planar silicon electronics and extendable to the 10-nm scale using crossed-nanowire architectures. These achievements, together with the recent advance in synthesis techniques allowing assembly of group IV, II–VI and III–V nanowires, hold great promise for the development of next-generation nanoelectronics and optoelectronics [24]. Simultaneously, the high degree of freedom in nanowire growth and device engineering creates new opportunities for the fabrication of controlled 1D systems for low-temperature applications and fundamental science. Quantum confinement and single-electron control have been achieved in a variety of single-nanowire devices [25]. Incorporation of magnetic semiconductor nanowires within nanodevices will be the first step towards 3D architectures of novel spintronic microchips [23]. Furthermore, nanowires provide an excellent opportunity to study the role of dimensionality and size in the magnetic properties of DMS materials. In this review, we focus on recent advances in the synthesis of DMS nanowires as well as discussing the structural, optical and magnetic properties of these materials.

2 II–VI DMS nanowires

II–VI semiconductor nanowires (NWs) such as CdS, CdSe and ZnS have been extensively studied due to their unique optical properties [26]. Doping such NWs with transition-metal ions will, in particular, allow an additional control of their optical properties by the magnetic field. The successful incorporation of transition-metal ions such as Mn within II–VI semiconductor nanowires was first reported by Froba, Klar and co-workers [27–29]. These nanowires were synthesized in the form of arrays within a MCM-41 mesoporous silica template by passing H_2S gas over a mixture of $Cd(OOCCH_3)$ and $Mn(OOCCH_3)$ adsorbed in the pores of the template. Electron paramagnetic resonance (EPR) results of these nanowires were comparable to those of exchange-coupled Mn^{2+} in chalcogenide mixed crystals. X-ray diffraction (XRD) and Raman spectra collected at room temperature suggested that the $Cd_{1-x}Mn_xS$ nanowire arrays had a wurtzite crystal structure [28] while EPR data collected at 4 K suggested a zincblende-like structure [27]. Moreover, the EPR data indicated that, with increasing Mn concentration, 1.5% to 5%, the zincblende structure undergoes a phase transformation to form the wurtzite structure. It should however be noted that electron-structure calculations on CdS clusters have indicated that wurtzite and zincblende structures are almost energetically degenerate, and thus formation of a particular crystal structure would be highly dependent on both the preparation process and the size of the nanostructure [30]. Extended absorption fine edge structure (EXAFS) measurements on $Cd_{1-x}Mn_xS$ nanowire arrays clearly indicated that Mn^{2+} ions occupy substitutional sites in the CdS host lattice replacing the Cd^{2+} ions [29]. The photoluminescence (PL) results indicated a blue shift of more than 200 meV in the direct band gap of the nanowires as compared to the bulk [29]. In addition, an increase of the *p–d* exchange-induced band-gap bowing as a function of Mn concentration was also observed. This effect was attributed to the modified positions of the *p*- and *d*-related bands in the band structure of the $Cd_{1-x}Mn_xS$ nanowire arrays. Superconducting quantum interference device (SQUID) [29] and EPR measurements [27, 29] indicated that the spin interactions between the $S = 5/2$ spins of the Mn^{2+} ions, which lead to the transition from the paramagnetic to the spin-glass phase for $0.20 < x < 0.45$ and to the transition from the paramagnetic to the antiferromagnetic phase for $x > 0.8$ in bulk $Cd_{1-x}Mn_xS$, are strongly suppressed in the nanowire arrays. The strong reduction of antiferromagnetic coupling between Mn^{2+} spins was further confirmed by temperature-dependent SQUID and EPR studies, whereby there is no evidence of phase transitions down to 2 K, with the Curie–Weiss parameter (Θ) in the paramagnetic region observed to be more than an order of magnitude smaller than in bulk $Cd_{1-x}Mn_xS$ [29]. $Zn_{1-x}Mn_xS$ nanowires were similarly synthesized within mesoporous silica powders using $Zn(OOCCH_3)$ as a source of Zn ions [31]. EXAFS analysis suggested that the Mn^{2+} ions randomly substitute Zn^{2+} ions in the ZnS host lattice. The above experimental procedure has been applied to form $Cd_{1-x}Mn_xS$ nanowire arrays within mesoporous silica thin films (MTFs) [32].

Recently, Na et al. have synthesized $Cd_{1-x}Mn_xS$ nanowires using a chemical vapour deposition (CVD) method where nanowire growth was seeded using Au nanoparticles deposited on a Si substrate [33]. Single-crystalline nanowires with an average diameter of 80 nm were obtained using this method. The nanowires exhibited either a [011] or a [010] growth direction as shown in Fig. 1. It was observed that the substitution of the Cd^{2+} ion with a smaller-radius Mn^{2+} ion results in a reduction of the lattice constants of CdS with increasing Mn-ion concentration. It was observed from the PL data that the *d–d* ($^4T_1 \rightarrow {}^6A_1$) transition, which is responsible for the Mn^{2+} emission at around 2.15 eV, is greatly enhanced at temperatures below 80 K. The decay time of this emission as estimated from the time-resolved PL spectrum was observed to decrease from 1 ms for $Cd_{0.9}Mn_{0.1}S$ nanowires to 0.55 ms for $Cd_{0.7}Mn_{0.3}S$ nanowires. The incorporation of Mn within CdS also significantly reduced the decay time for the band-edge emission from 590 ps for CdS nanowires to 22 ps $Cd_{0.7}Mn_{0.3}S$ nanowires. The most significant and technologically important aspect of this work, however, was the magneto-PL measurements which showed that it is possible to tune the optical properties of $Cd_{1-x}Mn_xS$ nanowires by applying a magnetic field. It was observed that with an applied magnetic field of 7 T the Mn^{2+} emission is suppressed while the donor–acceptor emission was enhanced, which suggests that the excitation of Mn^{2+} involves an energy-transfer process from the band excitons.

Radovanovic et al. have developed a new general approach for the synthesis of Mn-doped II–VI nanowires based on the metal-nanocluster-catalysed vapour–liquid–solid (VLS)

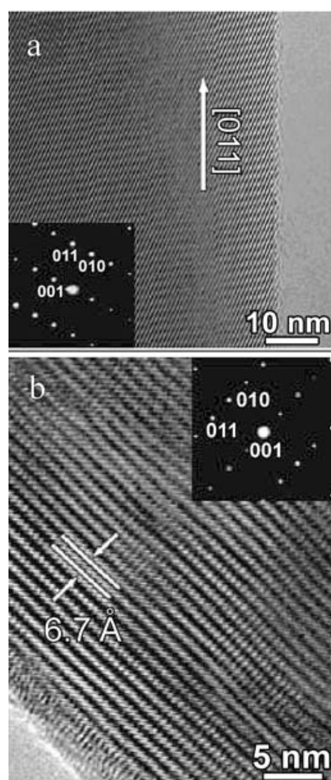

FIGURE 1 Atomic-resolved transmission electron microscope image of $Cd_{0.7}Mn_{0.3}S$ nanowires grown in the (**a**) [011] and (**b**) [010] growth directions. Reproduced with permission from J. Phys. Chem. B **110**, 6699 (2006). Copyright 2006, American Chemical Society

method [34]. Those authors first synthesized CdS and ZnS nanowires by employing a gold-nanocluster-catalysed VLS growth method and using single-source precursors such as $Cd(S_2CNEt_2)$ and $Zn(S_2CNEt_2)$. A shell layer was grown over the nanowires using a mixture of $Cd(S_2CNEt_2)$ and $Mn_2(CO)_{10}$ or $Zn(S_2CNEt_2)$ and $MnCO_3$ as precursors. The doping concentration was varied by changing the Mn/Cd or Mn/Zn precursor concentration. The shell growth was followed by annealing of the nanowires at 250 °C to obtain a uniform distribution of Mn ions within the nanowire. Energy-dispersive X-ray (EDX) measurements indicated that the Mn ions were distributed homogeneously throughout the nanowire and were not localized in an outer shell (Fig. 2).

Ge et al. reported a halide-transport CVD method to synthesize $Zn_{1-x}M_xS$ (M = Co, Mn or Cu) nanobelts and nanowires in which metal halides such as $MnCl_2$, $CoCl_2$ and $CuCl_2$ are used as a source of dopant ions [35]. The reactions were carried out by heating zinc and sulphur powders along with a metal halide at temperatures of 700–850 °C in an inert atmosphere. The morphology of the nanomaterial depended on the Zn/M^{2+} ratio; for example, 50–70 nm wide nanobelts with typical lengths in the range of ten to several hundreds of microns were formed when a Zn/Mn^{2+} ratio of 4 : 1 was used, while formation of both wire-like and ribbon-like nanostructures was observed at a Zn/Mn^{2+} ratio of 8 : 3. However, when a Zn/Mn^{2+} ratio of 2 : 1 was used, only nanowires with a diameter of 500 nm were observed. It was thus shown that it may be possible to control the morphology of the product by controlling the amount of dopant ion used. The change

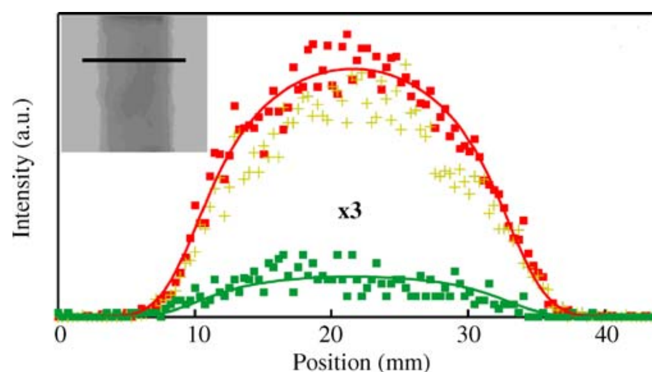

FIGURE 2 EDX line scans for the nanowire shown in the *inset*, with Cd, S and Mn data plotted as *red dots*, *yellow crosses* and *green dots*, respectively. The *red* and *green solid lines* through the data are fits to the experimental data for Cd and Mn, respectively. Reproduced with permission from Nano Lett. **5**, 1407 (2005). Copyright 2005, American Chemical Society

in morphology with Zn/Mn ratio is illustrated in Fig. 3. The room-temperature PL spectra of the nanobelt samples showed two peaks, one at 454 nm attributed to ZnS with a second at 572 nm that was attributed to the transition from ${}^4T_1 \rightarrow {}^6A_1$ states within the Mn centre. In the case of the pure nanowire samples the transition within the Mn centre was shifted to 574 nm. Those authors have attributed this small shift of 2 nm either to a possible MnS secondary phase formation where the Mn occupies an octahedral site instead of a tetrahedral site or to a radiation-less energy transfer in Mn clusters, where an exchange mechanism leads to the excited Mn^{2+} ion which resonantly transfers its energy to its neighbours until a low-energy centre is encountered. Although these explanations cannot be discounted, it is more than likely that a shift of 2 nm in the emission wavelength could be due to the different morphologies of the nanostructures.

3 Oxide-based DMS nanowires

In addition to metal sulphides, metal oxide nanowires such as ZnO have also been doped with transition metals such as Mn [36], Co [37] and Ni [37] in order to form DMS materials. Well-defined doping and defect chemistries, suitability for transparent high-power, high-temperature applications and the ability to emit spontaneously at ultraviolet wavelengths combine to make ZnO attractive for many potential device applications. For spintronics applications, the relatively long room-temperature spin-coherence time of n-type ZnO is advantageous [38]. Additionally, the potential to generate both p- and n-type ZnO of low resistivity makes bipolar spintronics based on ZnO a realistic possibility, and reports of both hole- [39] and electron-mediated [40] ferromagnetism in ZnO DMSs are encouraging. $Zn_{1-x}M_xO$ (M = Mn, Co, Ni) nanowires have been synthesized using both high-temperature CVD methods [36, 41, 42] as well as low-temperature solution-phase methods such as electrodeposition techniques [37, 43]. The magnetic properties of these materials are particularly interesting; for example, whilst Mn-doped ZnO nanowires exhibit a Curie temperature in the range of 37–44 K [36, 41, 42], doping with Co and Ni leads to nanowires which exhibit room-temperature ferromagnetism [37, 43]. It should be noted that Yu and co-workers

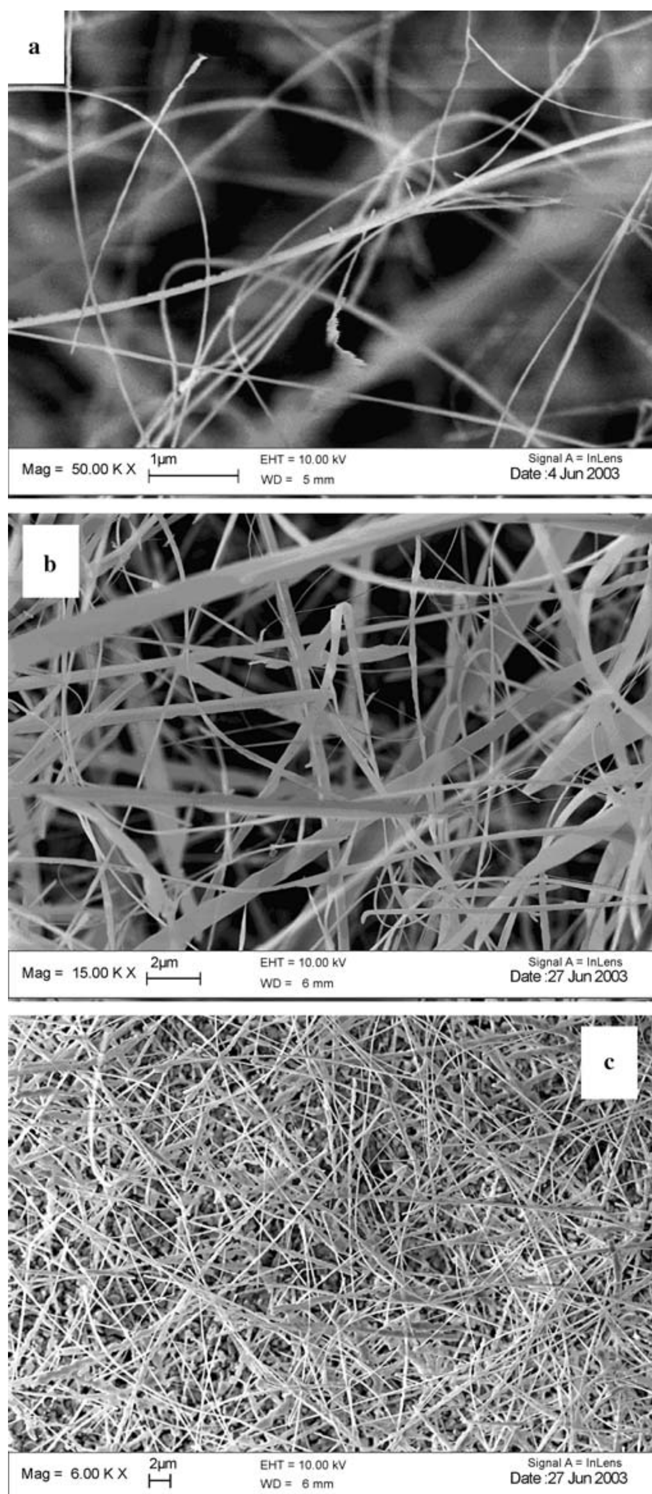

FIGURE 3 Scanning electron microscope images of the $Zn_{1-x}Mn_xS$ nanowires obtained from different Zn:Mn ratios. (**a**) Zn/Mn = 4/1, (**b**) Zn/Mn = 8/3, (**c**) Zn/Mn = 2/1. Reproduced with permission from Adv. Funct. Mater. **15**, 303 (2005). Copyright 2005, Wiley-VCH Verlag GmbH & Co

did not find any evidence for the presence of Mn_3O_4, which has a T_c of 42 K, in spite of detailed XRD, EDX, Raman and PL measurements [36, 41]. Generally, a high-temperature ($T_c > 300$ K) ferromagnetism in ZnO DMSs is intimately related to the electronic structures of the magnetic impurity ions as shown by electronic absorption, magnetic circular dichroism and photocurrent action spectroscopies [44]. The opposite polarities predicted and observed for ferromagnetic Co^{2+}:ZnO (n-type) and Mn^{2+}:ZnO (p-type) are of particular interest and allow a precise chemical engineering of the magnetic properties.

It appears significant that while a relatively low-temperature method such as electrodeposition has been used to synthesize $Zn_{1-x}Co_xO$ nanowires, high-temperature CVD methods have been used to synthesize $Zn_{1-x}Mn_xO$ nanowires. Growth conditions are known to affect the structural properties of materials; for example, high-temperature methods usually yield highly crystalline materials compared to low-temperature processes. The distribution of dopant ions within the lattice is also likely to be affected by the synthesis process. The difference in T_c between $Zn_{1-x}Co_xO$ and $Zn_{1-x}Mn_xO$ could be explained on the basis of different synthesis methods used. In order to test this hypothesis, however, the synthesis of $Zn_{1-x}Mn_xO$ nanowires by low-temperature methods such as electrodeposition is required as well as the synthesis of $Zn_{1-x}Co_xO$ nanowires using high-temperature CVD methods. It is also quite likely that the difference in electronic configuration of the dopant ion, i.e. d^5 for Mn^{2+} as against d^7 for Co^{2+}, plays a role in determining T_c of these nanowires.

Recently, the fabrication of a Co-doped TiO_2 nanowire based field effect transistor (FET) has been reported [45]. Poly(3,4-ethylenedioxythiophene) (PEDOT) nanowires were used as suspended templates for the growth of sputter-coated, Co-doped TiO_2 nanowires. The nanowires were individually suspended between Nb electrodes as shown in Fig. 4. Electrical transport measurements showed that a negative gate bias (V_g) reduces the current while a positive gate bias increases the current. An increase of the channel current (I_{sd}) at a positive gate voltage is a characteristic of an n-channel FET. The Co-doped TiO_2 nanowire based FET exhibited a relatively low transconductance (0.2×10^{-6} A/V) compared to other nanowire-based FETs [46]. However, a study of its magneto-transport properties is critical before this device can be used in spintronic devices.

A FET based on individual $ZnO/Zn_{1-x}Co_xO$ core–shell nanocables has very recently been reported [47]. These n-type FET devices showed a negative magnetoresistance (MR) of 2.1% at 13 K and 1.1% at 20 K. At temperatures above 30 K no obvious change in resistance with magnetic field was observed.

4 III–V DMS nanowires

Theoretical studies based on Zener-model calculations have predicted a $T_c > 300$ K for bulk $Ga_{1-x}Mn_xN$ [5] and studies of thin films have also reported a T_c in the range of 250–370 K [7]. Although III–V DMS bulk materials have been extensively studied and modelled, there have been very few reports of the synthesis of nanowires. Deepak et al. first reported the synthesis of III–V DMS nanowires [48], whereby they used single-walled (SWNT) and multi-walled (MWNT) carbon nanotube bundles as templates within which crystalline $Ga_{1-x}Mn_xN$ nanowires were formed. Although extensive magnetic characterization of these nanowires was not carried out, they were found to be ferromagnetic with a T_c

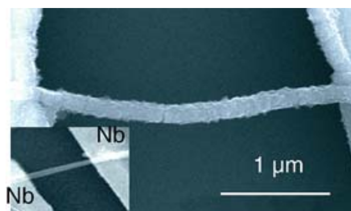

FIGURE 4 A suspended Co-doped TiO_2 nanowire junction between Nb electrodes. *Inset figure* represents the suspended molecular template junction before fabrication of the Co-doped TiO_2 nanowire. Reproduced with permission from Appl. Phys. Lett. **86**, 033 110 (2005). Copyright 2005, American Institute of Physics

of approximately 325 K comparable to that obtained for thin films and predicted for bulk materials. A coercivity as high as 1400 Oe for 5% Mn doped nanowires having a mean diameter of 25 nm was observed, a value which is much higher than that reported for thin films (100–500 Oe) [7].

More recently, the magnetotransport properties of single-crystalline $Ga_{1-x}Mn_xN$ nanowires have been reported [49, 50]. Choi et al. have used a nickel-catalysed chloride-transport CVD method to synthesize $Ga_{1-x}Mn_xN$ nanowires [49]. These nanowires had diameters in the range of 10–100 nm with lengths of tens of micrometres. The average Mn concentration was determined to be 7% and the Mn ions were found to be homogeneously distributed within the nanowire lattice. PL and electron energy loss spectroscopy (EELS) unambiguously proved that the Mn ions exist as Mn^{2+} within the GaN lattice, which is consistent with the Mn oxidation state observed in thin films of $Ga_{1-x}Mn_xN$ [51]. Coercive fields as obtained from SQUID measurements were observed to be 80 Oe at 5 K and 40 Oe at 300 K. Additionally, the $Ga_{1-x}Mn_xN$ nanowires exhibited a negative MR of 1.4% at 2 K and 0.4% at 250 K in an applied magnetic field of 9 T. A similar MR effect has been observed in $Ga_{1-x}Mn_xN$ thin films [52].

Han et al. have also reported ferromagnetic ordering at room temperature as well as a negative MR in single-crystalline $Ga_{1-x}Mn_xN$ nanowires [50]. These nanowires were synthesized using a CVD method in the absence of a catalyst. A coercivity of 100 Oe and a negative MR of 2.5% at 5 K were estimated for the nanowires synthesized using this technique. The slightly higher MR and coercivity could be explained on the basis of the size distribution of the nanowire diameter. The diameters of the nanowires synthesized by Han et al. were in the range of 40–70 nm as compared to 10–100 nm for those reported by Choi et al. The narrow size distribution may play a role in the enhanced coercivity, which increases by 25%, and in the MR, which shows an increase of about 40%. It is also possible that the different synthesis conditions used to grow the nanowires influence the magnetoresistive properties. However, although an increase in MR and coercive field has been observed in both works, the MR transition temperature (T_{MR}) was estimated to be 150 K [50] as compared to 250 K for that reported by Choi et al. [49]. The decrease in T_{MR} could be attributed to a smaller Mn content (5%) in these nanowires. Although some differences in magnetic properties of $Ga_{1-x}Mn_xN$ nanowires reported in [50] and [49] are observed, they could be easily explained on the basis of Mn concentration and size distribution. However, the observations of Deepak et al. [48] are dramatically different from those reported in [49] and [50]. A coercivity of 1400 Oe for 25-nm nanowires as reported by Deepak et al. seems extraordinarily high when compared to thin films and other $Ga_{1-x}Mn_xN$ nanowires. The nanowires in [48], which are synthesized in SWNT templates, have a very narrow size distribution (20–25 nm) but the ones synthesized in MWNTs have diameters in the range of 50–75 nm. A high coercivity in the range of 620–970 Oe for the nanowires synthesized within MWNTs thus cannot be explained on the basis of size distribution. It should be noted that the MWNTs and SWNTs used as templates for the synthesis of $Ga_{1-x}Mn_xN$ nanowires are in fact removable templates, which are calcined during the course of nanowire formation due to the high temperature (950 °C) used in the synthesis; hence, a small amount of co-doping with carbon cannot be entirely ruled out, which might explain the increased coercivity observed in these nanowires. An enhancement of magnetic properties as reflected by an increase in T_c has been observed in $Ga_{1-x}Mn_xAs$ thin films when co-doped with carbon [53]. Carbon was shown to occupy the arsenic site and acts as a shallow acceptor, thus increasing the carrier concentration. It is possible that a similar mechanism leads to an increased coercivity in the $Ga_{1-x}Mn_xN$ nanowires synthesized by Deepak et al.

In order to determine the role of the carrier type and concentration, Choi et al. [49] prepared a $Ga_{1-x}Mn_xN$ nanowire based field effect transistor (FET) structure. A low resistivity of $1.1 \times 10^{-2}\ \Omega\,cm$ along with a weak gating effect indicated a high carrier concentration within the $Ga_{1-x}Mn_xN$ nanowires. Further evidence for a high carrier concentration was provided by the carrier mobility, which was estimated to be $70\ cm^2\ V^{-1}\ s$, which is low compared to that of thick films of $Ga_{1-x}Mn_xN$ [54]. A carrier concentration of $2 \times 10^{19}\ cm^{-3}$ was estimated for these $Ga_{1-x}Mn_xN$ nanowires, which is about 10 times lower than that assumed in the theoretical model for a room-temperature T_c [5]. A decrease in conductivity with increasing gate voltage was observed from the I–V curves, which suggests the presence of p-type carriers within the nanowires and which possibly indicates that in single-crystalline $Ga_{1-x}Mn_xN$ nanowires holes are responsible for both charge transport and ferromagnetic interactions. This supports the Zener model of hole-mediated room-temperature ferromagnetism for $Ga_{1-x}Mn_xN$ [5]. A light-emitting diode (LED) structure based on $Ga_{1-x}Mn_xN$ nanowires was fabricated by growing these nanowires on a SiC substrate using a Ni catalyst [49], a schematic of which is shown in Fig. 5a. Figure 5b shows the transport measurements of these nanowire-based LEDs showing current-rectification characteristic of p–n diodes. Electroluminescence (EL) measurements showed an emission peak centred at 430 nm, which was consistent with the PL of $Ga_{1-x}Mn_xN$ nanowires.

Similarly, $Ga_{1-x}Mn_xP$ nanowires having diameters in the range of 10–100 nm have been synthesized by a CVD process using Au nanoparticles as a catalyst [55]. Some of the nanowires exhibited a periodically bumpy surface morphology as can be clearly seen in Fig. 6a. The nanowire growth direction was along the [111] plane with a number of defect lines along the same direction as illustrated in Fig. 6b. It was observed that Mn was mainly concentrated in the outer layers of the nanowire. The Mn content along the cross sec-

tion of the nanowire varied from 20% in the outer layers to 1% in the core, as suggested by the elemental mapping of a cross section of an individual nanowire shown in Fig. 6c. The higher amount of Mn in the outer layers was attributed to the relatively lower solubility of Mn in the Au nanoparticles as compared to Ga, resulting in the excess Mn vapour that cannot dissolve in Au depositing as amorphous oxide layers. SQUID measurements indicate the presence of soft ferromagnetism with a T_c of 330 K. Although this transition temperature is higher than that predicted for bulk p-type $Ga_{1-x}Mn_xP$ ($T_c = 100$ K) [5], it is comparable to that reported for GaP thin films ($T_c \approx 320$ K) [56]. Variations of the magnetic properties of the nanowires compared to the GaMnP thin films could be attributed to an inhomogeneous distribution of the Mn ions within the nanowires. In the case of $Ga_{1-x}Mn_xP$ thin films it was observed that increasing the Mn content from 3% to 5% causes a decrease of the magnetic ordering [56]. A detailed study of the magnetic properties of $Ga_{1-x}Mn_xP$ nanowires with varying Mn content is required to confirm this explanation. A negative MR of 5% was observed in these nanowires at 20 K as compared to 0.35% in the case of $Ga_{1-x}Mn_xP$ thin films. The extraordinarily large MR value in the case of $Ga_{1-x}Mn_xP$ nanowires has been attributed to an efficient alignment of spins along the long axis of the nanowires. However, the contribution of amorphous Mn oxides present in the outer layers of the nanowires cannot be completely ruled out [57].

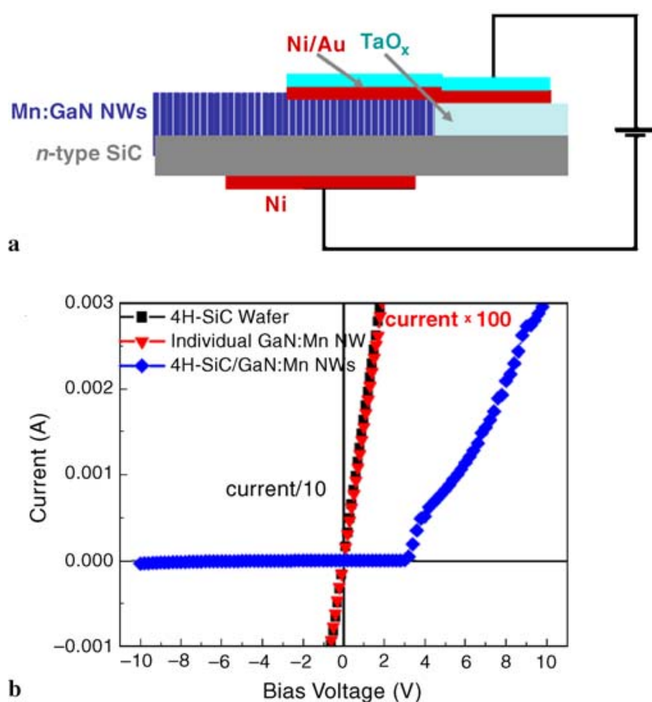

FIGURE 5 (**a**) Schematic illustration of the LED structures. To avoid mechanical failure in the measurements, a TaO_x film was deposited in a small area and metal (Ni/Au) was then evaporated on the nanowire tips through a shadow mask, resulting in a continuous contact layer on the nanowires and TaO_x insulator. Measurements were carried out by probe contact on the metal layer above the TaO_x layer. (**b**) I–V behaviour of n-SiC substrate/$Ga_{1-x}Mn_xN$ nanowire junction. Reproduced with permission from Adv. Mater. **17**, 1351 (2005). Copyright 2005, Wiley-VCH Verlag GmbH & Co

5 Group IV DMS nanowires

As compared to II–VI and III–V DMS nanowires, there have been very few reports of group IV nanowires. This is rather surprising considering the importance of group IV materials such as Si and Ge in state of the art microelectronic applications. At UCC and NPL we have reported the synthesis and ferromagnetic ordering at room temperature in $Ge_{1-x}Mn_x$ nanowire arrays within anodic aluminium oxide (AAO) membranes [58, 59]. This is the first report of the synthesis of group IV DMS nanowires. We have used a supercritical fluid (SCF) deposition method to fabricate high-density arrays of $Ge_{1-x}Mn_x$ ($x = 1\%–5\%$) nanowires with diameters of 35, 50 and 60 nm. The SCF deposition method ensures complete filling of the porous AAO membranes due to the high diffusivity and low viscosity of SCFs [60, 61]. The presence of a crystalline host Ge lattice was confirmed by XRD, while the local structural and chemical environment was probed using EXAFS and X-ray absorption near edge structure (XANES) measurements. EXAFS results as shown in Table 1 suggest that Ge is surrounded by a shell of O atoms at a distance of 1.74 Å, which implies that the Ge atoms are anchored to O atoms on the AAO membrane. The next-nearest atoms to Ge were other Ge atoms at a bond distance of 2.44 Å, corresponding to the Ge–Ge bond distance in the Ge nanowires. Mn atoms were surrounded by a shell of O atoms at a distance of 2.11 Å. The next-nearest neighbour of Mn was Ge at a distance of 3.03 Å. The third-nearest neighbour of Mn was also Ge at a distance of 4.06 Å. It was thus shown that Mn is surrounded by O and Ge atoms rather than other Mn atoms, which implies that the Mn atoms are spatially separated from each other. Although from the EXAFS data it was not possible to determine the precise position of Mn in the nanowire–AAO structure, it confirmed the absence of secondary phases of ferromagnetic alloys such as Ge_3Mn_5, Ge_5Mn_3 and Ge_8Mn_{11}. XANES and X-ray photoelectron spectroscopy (XPS) strongly suggested that Mn exists predominantly in the +3 oxidation state. Although single-crystalline nanowires would possibly be desirable in order to minimizes both electron and spin scattering, it should be noted that $Ge_{1-x}Mn_x$ nanowires obtained by the SCF method are polycrystalline in nature.

Well-pronounced room-temperature ferromagnetic properties, i.e. strongly non-linear $M(H)$ curves with a low field saturation and hysteresis, as well as a non-zero remanence magnetization and coercivity, were observed in nanowires having a mean diameter of 35 nm at concentrations $x \geq 1.5\%$. The magnetization saturation was of the order of $M_s = 10–14$ emu cm^{-3}. The smallest difference in the shape and saturation value of the room- and low-temperature curves for the nanowires with $x = 3\%$ possibly indicates that this sample has the highest T_c. Both ferromagnetic and paramagnetic phases were observed in the nanowire at a Mn concentration of 1%. The concentration dependence of the coercive field revealed a maximum at a Mn concentration of 3%. Typically, a coercivity of 30–60 Oe was observed for these nanowires depending on the Mn concentration. The diamagnetic behaviour of the reference sample (undoped Ge nanowires) together with convincing structural results from

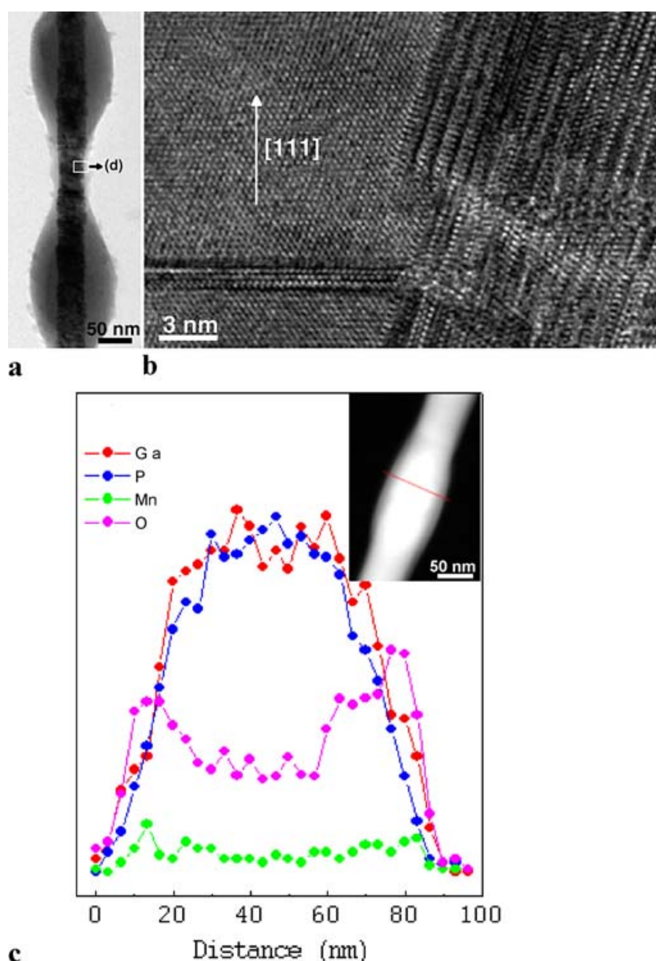

FIGURE 6 (**a**) Detailed feature of a bumpy Mn-doped GaP nanowire and (**b**) its atomic-resolved electron microscope image showing a number of defect lines along the [111] direction. (**c**) Elemental mapping cross section showing Mn and O concentrations at the outer layers. The corresponding scanning transmission electron microscope image is shown in the *inset*. Reproduced with permission from J. Phys. Chem. B **109**, 9311 (2005). Copyright 2005, American Chemical Society

EXAFS measurements proves that the observed soft ferromagnetism originates from Mn ions diluted in the Ge matrix, i.e. $Ge_{1-x}Mn_x$ nanowires exhibit a DMS type of ferromagnetic ordering.

The small diameters of the nanowires may cause substantial interfacial strain, which leads to a distortion of the crystal lattice at the nanowire–AAO interface. Such strain will unavoidably produce an increase of interfacial magnetic anisotropy which masks the magnetic properties of the system. In order to investigate qualitatively the effect of the strain, $Ge_{1-x}Mn_x$ nanowires with a larger diameter, $d = 60$ nm, having a lower surface–volume ratio were studied. The magnetization curves as shown in Fig. 7 are typical of a ferromagnetically ordered medium, i.e. saturated at $H_s = 2–7$ kOe, and had a rectangular shape and a large coercive field, $H_c \approx 600$ Oe, even at room temperature. The saturation magnetization decreased with increasing temperature and at room temperature reached only about 70% of its initial low-temperature value, while the overall type of the hysteresis curve still remained ferromagnetic. The shape of the M vs. H curves was about the same in the temperature range of $T = 4–300$ K, whereas it was less steep in the low and intermediate fields ($0 < H < 4$ kOe) at $T = 1.8$ K. Thus, reducing the interface-related strain allowed us to readily observe room-temperature ferromagnetism even at the lowest concentration of Mn.

A Curie temperature above room temperature was observed in this study even at the lowest Mn concentration used for $Ge_{1-x}Mn_x$ ($x = 1\%$) nanowire arrays. It should be noted that, despite the relatively high growth temperatures used in the synthesis of the $Ge_{1-x}Mn_x$ nanowire arrays, $T = 773$ K [58, 59], the SCF fabrication method allows the preparation of DMS materials which are free from undesirable phase-separation and Mn-clustering effects. Although the formation of secondary phases is commonly observed in $Ge_{1-x}Mn_x$ films deposited by molecular beam epitaxy (MBE) even at significantly lower temperatures, the structural analysis of our samples did not reveal the presence of any GeMn alloys at $x < 5\%$. It is possible that the small nanowire diameters considerably reduce the probability of clustering. A similar result was achieved in MBE-grown samples by reducing the film thickness [62]. It could be argued that EXAFS measurements may not be sensitive enough to detect small particles of phase-separated GeMn ferromagnetic alloys. However, ferromagnetic particles, if any, must be very small indeed to escape detection. As ultra-small particles would normally be expected to display superparamagnetic properties [63], they are unlikely to be responsible for the ferromagnetism observed in the $Ge_{1-x}Mn_x$ nanowire array samples.

In previous studies of $Ge_{1-x}Mn_x$ thin films [14], the oxidation state of the Mn in the Ge lattice was commonly observed to be +2. Although a magnetic moment of $5\,\mu_B$ is expected for a Mn^{2+} ion in the substitutional site in a Ge lattice, electronic structure calculations [14] have shown the strong hybridization between d states of Mn and p states of Ge, which causes the reduced value of the magnetic moment of about $3\,\mu_B$ per Mn atom. It should be noted that in our samples the majority of manganese atoms were in the ionized Mn^{3+} state, which is characterized in its ground state (i.e. without taking into account hybridization effects) by lower spin, $S = 2$, and reduced magnetic moment ($4\,\mu_B$ per atom) compared with the Mn^{2+} state. Although the loss of a d elec-

Sample	T_1	R_1 (Å)	T_2	R_2 (Å)	T_3	R_3 (Å)
Ge K-edge $Ge_{1-x}Mn_x$	O	1.746 ± 0.004	Ge	2.443 ± 0.005	–	–
Mn K-edge $Ge_{1-x}Mn_x$	O	2.117 ± 0.008	Ge	3.042 ± 0.021	Ge	4.064 ± 0.113

TABLE 1 Fitted data for Ge and Mn K-edge EXAFS measurements of $Ge_{0.99}Mn_{0.01}$ and $Ge_{0.99}Mn_{0.01}$ nanowire arrays. T_1, T_2 and T_3 represent the atom that best fits the EXAFS data. R_1, R_2 and R_3 are the corresponding distances from the central atom. Reproduced with permission from Chem. Mater. **17**, 3615 (2005). Copyright 2005, American Chemical Society

tron in this case should give rise to an orbital momentum, detailed calculations of the Mn^{3+} electronic structure in the Ge host are required in order to determine the total momentum of the Mn ions. In the concentration range of $1\% \leq x \leq 3\%$ the maximum saturation moment per Mn atom was about $1.8\,\mu_B$ at $T = 1.8$ K. As the temperature increases, the magnetic moment per Mn atom dropped to $1.0\,\mu_B$ at $T = 300$ K. The result was in good agreement with previous studies of $Ge_{1-x}Mn_x$ [14] and GaMnAs [64] thin-film samples. The observed low value of the magnetic moment might be explained by a generally reduced moment of Mn^{3+} ions as well as some amount of Mn ions being in a magnetically inactive state. Although EXAFS and XANES studies did not show manganese atoms in the next-neighbour positions, the formation of antiferromagnetically coupled nearest-neighbour dimers cannot be entirely excluded within an uncertainty of the experimental technique. In such a configuration magnetic moments of individual ions are mutually compensated and the dimer is magnetically neutral. Thus, in this situation both Mn ions would appear magnetically inactive. It should be noted that a significant change in the hybridization level between d orbitals of Mn and p orbitals of the Ge host might be typical for the ionized Mn^{3+} state. In particular, weaker hybridization will lead to a weaker coupling between Mn ions and holes, which would make carriers less localized and favour longer-range interactions. Overall, it may cause room-temperature ferromagnetism as observed in $Ge_{1-x}Mn_x$ nanowires. The main question arising from the experimental data is what makes the Curie temperature in $Ge_{1-x}Mn_x$ nanowires so high with respect to that of the bulk materials and films. Generally, several theoretical models have been used to explain a concentration dependence of T_c. In particular, models based both on exchange interaction between carriers and localized spins [5] and using ab initio calculations [65] predicted a T_c much lower than we observe experimentally in $Ge_{1-x}Mn_x$ nanowires. However, Park et al. [14]

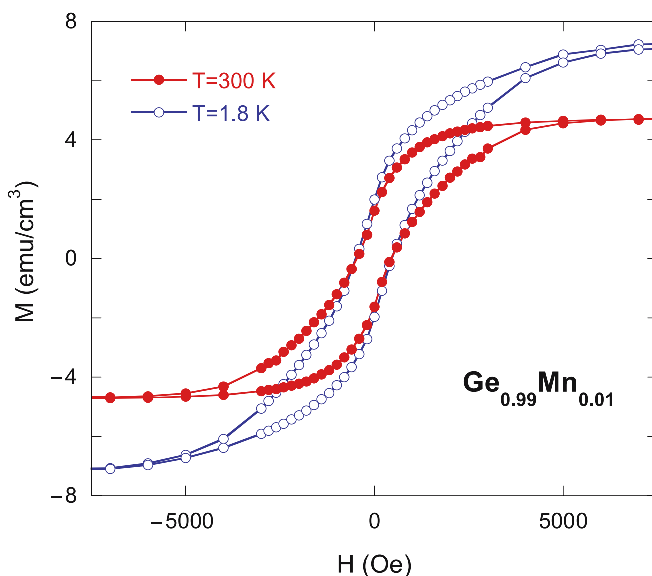

FIGURE 7 Hysteresis curves of $Ge_{0.99}Mn_{0.01}$ nanowires of diameter 60 nm. Reproduced with permission from Phys. Rev. B **72**, 094 415/1 (2005). Copyright 2005, American Physical Society

used a combination of electronic structure calculations based on a density-functional theory and a percolation approach to obtain a $T_c = 300$ K for $x = 2\%$. Although those authors were not able to explain their own experimental results, it is the only approach which indicates a possibility of room-temperature ferromagnetism in group IV semiconductors. As $Ge_{1-x}Mn_x$ is a p-type semiconductor, the hole concentration plays an essential role in the mediation of ferromagnetic ordering between localized spins of Mn atoms. Recent work on p-type semiconductors showed that T_c could be increased up to and beyond room temperature if the carrier concentration is significantly raised [53, 66]. It was shown that co-doping of GaAs:Mn by carbon leads to enhanced magnetic properties of the material, e.g. non-zero remanent magnetization was observed up to 280 K [53]. As carbon-containing precursors (diphenylgermane and dimanganese decacarbonyl) were used during the nanowire fabrication, the possibility of carbon penetration into the nanowire and especially its presence at the interface is relatively high. A hole-enriched $Ge_{1-x}Mn_x$ might demonstrate enhanced magnetic properties due to a co-doping effect in agreement with the references above. Assuming the presence of co-dopant, the existence of single-phase ferromagnetic ordering at the lowest Mn concentration can also be attributed to a relatively high carrier density which only partly originates from Mn doping. As the presence of oxygen in $Ge_{1-x}Mn_x$ nanowires was proved by EXAFS, its influence on the magnetic properties cannot be excluded. It has been observed that in wide-band GaN:Mn semiconductors addition of oxygen (8%) leads to a significant enhancement of the magnetic moment [67]. In strongly confined $Ge_{1-x}Mn_x$ nanowires the surface–volume ratio of atoms is significantly increased compared with thin films and bulk samples. This ratio is even higher for the dopant atoms, as an enhanced Mn concentration in the nanowire shell was observed. As the host lattice is distorted in the vicinity of the membrane, the symmetry of the Mn-atom environment at the interface does not correspond to that in the inner part of the nanowire. Thus, the AAO–nanowire interface should notably influence the electronic and magnetic properties of Mn at the nanowire shell and may lead to the high value of the Curie temperature. A concentration-dependence study reveals that the ferromagnetic behaviour is most pronounced for samples with intermediate Mn concentration, $x = 1.5$ and 3%. This is consistent with results of others [14], where, despite an overall rather low Curie temperature, the maximum of T_c was reached at $x = 3.5\%$. At the same time, D'Orazio et al. [62] demonstrated a very similar concentration dependence with a maximum of magnetic performance at the intermediate concentration range followed by a total collapse of ferromagnetism at $x = 5.5\%$. These results are also consistent with earlier studies [14, 65], where reduction of the pair-exchange interaction with increasing concentration of the Mn atoms was observed. In the case of nanowires of small diameter and low Mn concentration, ferromagnetic ordering is less likely in the nanowire core as Mn ions are spaced further apart there. Thus, the central part of the nanowire is assumed to be paramagnetic due to localized magnetic ions, whereas a ferromagnetic ordering takes place in the narrow region at the border with the AAO membrane. While in the nanowire core Mn ions are likely to occupy a substitutional position, the energy of

formation of both substitutional and interstitial defects is the same on the Ge interface [68]. In this case, the initially low concentration of carriers could be further decreased by Mn interstitial defects. Such defects act as donors, compensating a fraction of the free holes. As either the concentration of Mn and carriers or the nanowire diameter increases, it becomes sufficient to overcome the reducing influence of interfacial defects.

Generally, the decrease of the Curie temperature with increasing mean concentration of dopants in thin films and bulk samples is believed to be connected with either the hole-compensation effect or the clustering of dopants. Thus, the observed high T_c suggests suppression of both mentioned effects in the nanowire geometry.

The synthesis of $Ge_{1-x}Mn_x$ nanowires as small as 5 nm in diameter has recently been reported [69]. These nanowires were synthesized using a CVD method with Au nanoparticles acting as nucleating centres. Although extensive magnetic characterization of these nanowires is required, their magnetic properties might throw light on the possible magnetic interactions taking place in size-quantized Ge-based DMS nanowires.

6 Conclusions

The fabrication of practical spintronic devices based on DMS nanowires would require (1) available spin-polarized carriers at room temperature; (2) compatibility with conventional CMOS technology; (3) ferromagnetism which is electrically tunable, i.e. interaction of electrical carriers with the magnetic subsystem; (4) high carrier mobility; and (5) retention of semiconducting properties when doped. Although a majority of studies of DMS materials have focused on thin films and bulk materials, significant progress has been made towards the synthesis of DMS nanowires. However, synthetic approaches such as systematic co-doping with either non-magnetic or magnetic ions, which have yielded interesting properties in bulk DMS materials, have not yet been employed in the synthesis of DMS nanowires. It would be possible to vary the carrier concentration in the system without disturbing the magnetic ion concentration by doping with a non-magnetic ion such as carbon and boron while co-doping using two different elements such as Mn and Co in the Ge host, which can compensate for the effects of lattice strain caused by the doping species and may eventually lead to highly doped magneto-electronic materials. Investigation of magnetotransport and magnetoresistive properties is critical if DMS nanowires are to be incorporated into devices. However, with the exception of $Ga_{1-x}Mn_xN$ nanowires, very little is known about magnetotransport properties of DMS nanowires. Although extensive magnetic and magnetoresistive characterization has been carried out on $Ga_{1-x}Mn_xN$ nanowires, the measurements have been performed on individual nanowires rather than nanowire arrays which are required for a large-scale device fabrication. Even though measurements of magnetotransport properties of arrays may pose significant challenges related to the electrical contact to the DMS nanowires, recent progress in contacting semiconductor nanowires [60] suggests that the problems could be overcome.

The incorporation of DMS nanowires within practical devices is as yet not realized, although there have been some successful attempts to fabricate FET devices using DMS nanowires such as $Ti_{1-x}Co_xO_2$, $Ga_{1-x}Mn_xN$ and $ZnO/Zn_{1-x}Co_xO$.

The fabrication of DMS nanowires having the desirable properties listed above may lead to a range of devices such as high-density magnetic memories, LEDs and FETs based on DMS nanowires and optical devices such as diodes and displays which can be operated by a magnetic field as well as spin-injection devices, e.g. amplifiers, frequency multipliers and square-law detectors based on 1D heterostructures [70]. Thus, for spintronics applications it is very advantageous to combine the desirable magnetic properties of DMS materials with a low dimensionality of nanowires. Such synergy provides both nanoscale lateral dimensions, which are extremely beneficial for miniaturization of devices, and alteration (often enhancement) of physical properties due to the strong confinement effect and the shape anisotropy.

ACKNOWLEDGEMENTS JDH is grateful to Prof. J. Fischer for the invitation to write this review. The authors acknowledge financial support from the Higher Education Authority and Science Foundation in Ireland, the QMP04.3.4 of the NMS Quantum Metrology Program and the NPL's Strategic Research Program.

REFERENCES

1 H. Ohno, H. Munekata, T. Penney, S. Von Molnar, L.L. Chang, Phys. Rev. Lett. **68**, 2664 (1992)
2 G. Schmidt, J. Phys. D **38**, R107 (2005)
3 A.H. MacDonald, P. Schiffer, N. Samarth, Nat. Mater. **4**, 195 (2005)
4 S.J. Pearton, M.E. Overberg, G.T. Thaler, C.R. Abernathy, J. Kim, F. Ren, N. Theodoropoulou, A.F. Hebard, Y.D. Park, Phys. Stat. Solidi A **195**, 222 (2003)
5 T. Dietl, H. Ohno, F. Matsukura, J. Cibert, D. Ferrand, Science **287**, 1019 (2000)
6 P. Sharma, A. Gupta, K.V. Rao, F.J. Owens, R. Sharma, R. Ahuja, J.M.O. Guillen, B. Johansson, G.A. Gehring, Nat. Mater. **2**, 673 (2003)
7 M.L. Reed, N.A. El-Masry, H.H. Stadelmaier, M.K. Ritums, M.J. Reed, C.A. Parker, J.C. Roberts, S.M. Bedair, Appl. Phys. Lett. **79**, 3473 (2001)
8 S.J. Pearton, C.R. Abernathy, G.T. Thaler, R.M. Frazier, D.P. Norton, F. Ren, Y.D. Park, J.M. Zavada, I.A. Buyanova, W.M. Chen, A.F. Hebard, J. Phys.: Condens. Matter **16**, R209 (2004)
9 G.T. Thaler, R.M. Frazier, J. Stapleton, C.R. Abernathy, S.J. Pearton, J. Kelly, R. Rairigh, A.F. Hebard, J.M. Zavada, Electrochem. Solid State Lett. **7**, G34 (2003)
10 G.T. Thaler, M.E. Overberg, B. Gila, R. Frazier, C.R. Abernathy, S.J. Pearton, J.S. Lee, S.Y. Lee, Y.D. Park, Z.G. Khim, J. Kim, F. Ren, Appl. Phys. Lett. **80**, 3964 (2002)
11 S. Dhar, O. Brandt, A. Trampert, L. Daweritz, K.J. Friedland, K.H. Ploog, J. Keller, B. Beschoten, G. Guntherodt, Appl. Phys. Lett. **82**, 2077 (2003)
12 A.F. Hebard, R.P. Rairigh, J.G. Kelly, S.J. Pearton, C.R. Abernathy, S.N.G. Chu, R.G. Wilson, J. Phys. D **37**, 511 (2004)
13 J. Kudrnovsky, V. Drchal, I. Turek, L. Bergqvist, O. Eriksson, G. Bouzerar, L. Sandratskii, P. Bruno, J. Phys.: Condens. Matter **16**, S5571 (2004)
14 Y.D. Park, A.T. Hanbicki, S.C. Erwin, C.S. Hellberg, J.M. Sullivan, J.E. Mattson, T.F. Ambrose, A. Wilson, G. Spanos, B.T. Jonker, Science **295**, 651 (2002)
15 S. Cho, S. Choi, S.C. Hong, Y. Kim, J.B. Ketterson, B.-J. Kim, Y.C. Kim, J.-H. Jung, Phys. Rev. B **66**, 033 303/1 (2002)
16 H. Braak, R.R. Gareev, D.E. Buergler, R. Schreiber, P. Gruenberg, C.M. Schneider, J. Magn. Magn. Mater. **286**, 46 (2005)
17 F. Tsui, L. He, L. Ma, A. Tkachuk, Y.S. Chu, K. Nakajima, T. Chikyow, Phys. Rev. Lett. **91**, 177 203/1 (2003)
18 Y. Huang, X. Duan, Y. Cui, L.J. Lauhon, K.-H. Kim, C.M. Lieber, Science **294**, 1313 (2001)

19 M.T. Bjork, B.J. Ohlsson, C. Thelander, A.I. Persson, K. Deppert, L.R. Wallenberg, L. Samuelson, Appl. Phys. Lett. **81**, 4458 (2002)
20 X. Duan, Y. Huang, Y. Cui, J. Wang, C.M. Lieber, Nature (London) **409**, 66 (2001)
21 J.C. Johnson, H. Yan, R.D. Schaller, L.H. Haber, R.J. Saykally, P. Yang, J. Phys. Chem. B **105**, 11 387 (2001)
22 X.T. Zhou, J.Q. Hu, C.P. Li, D.D.D. Ma, C.S. Lee, S.T. Lee, Chem. Phys. Lett. **369**, 220 (2003)
23 Y. Wu, J. Xiang, C. Yang, W. Lu, C.M. Lieber, Nature **430**, 61 (2004)
24 Y. Xia, P. Yang, Y. Sun, Y. Wu, B. Mayers, B. Gates, Y. Yin, F. Kim, H. Yan, Adv. Mater. **15**, 353 (2003)
25 C. Thelander, H.A. Nilsson, L.E. Jensen, L. Samuelson, Nano Lett. **5**, 635 (2005)
26 X. Duan, C.M. Lieber, Adv. Mater. **12**, 298 (2000)
27 L. Chen, P.J. Klar, W. Heimbrodt, F. Brieler, M. Froba, H.A. Krug von Nidda, A. Loidl, Physica E **10**, 368 (2001)
28 L. Chen, P.J. Klar, W. Heimbrodt, F. Brieler, M. Froba, Appl. Phys. Lett. **76**, 3531 (2000)
29 F.J. Brieler, M. Froba, L. Chen, P.J. Klar, W. Heimbrodt, H.-A. Krug von Nidda, A. Loidl, Chem. Eur. J. **8**, 185 (2002)
30 J.-O. Joswig, M. Springborg, G. Seifert, J. Phys. Chem. B **104**, 2617 (2000)
31 F.J. Brieler, P. Grundmann, M. Froeba, L. Chen, P.J. Klar, W. Heimbrodt, H.-A. Krug von Nidda, T. Kurz, A. Loidl, J. Am. Chem. Soc. **126**, 797 (2004)
32 A.V. Kouzema, M. Froeba, L. Chen, P.J. Klar, W. Heimbrodt, Adv. Funct. Mater. **15**, 168 (2005)
33 C.W. Na, D.S. Han, D.S. Kim, Y.J. Kang, J.Y. Lee, J. Park, D.K. Oh, K.S. Kim, D. Kim, J. Phys. Chem. B **110**, 6699 (2006)
34 P.V. Radovanovic, C.J. Barrelet, S. Gradecak, F. Qian, C.M. Lieber, Nano Lett. **5**, 1407 (2005)
35 J.-P. Ge, J. Wang, H.-X. Zhang, X. Wang, Q. Peng, Y.-D. Li, Adv. Funct. Mater. **15**, 303 (2005)
36 Y.Q. Chang, D.B. Wang, X.H. Luo, X.Y. Xu, X.H. Chen, L. Li, C.P. Chen, R.M. Wang, J. Xu, D.P. Yu, Appl. Phys. Lett. **83**, 4020 (2003)
37 J.B. Cui, U.J. Gibson, Appl. Phys. Lett. **87**, 133 108 (2005)
38 S. Ghosh, V. Sih, W.H. Lau, D.D. Awschalom, S.-Y. Bae, S. Wang, S. Vaidya, G. Chapline, Appl. Phys. Lett. **86**, 232 507 (2005)
39 K.R. Kittilstved, N.S. Norberg, D.R. Gamelin, Phys. Rev. Lett. **94**, 147 209 (2005)
40 M. Venkatesan, C.B. Fitzgerald, J.G. Lunney, J.M.D. Coey, Phys. Rev. Lett. **93**, 177 206 (2004)
41 Y.-Q. Chang, X.-Y. Xu, X.-H. Luo, Y. Long, R.-C. Ye, Chin. Phys. Lett. **22**, 991 (2005)
42 J.J. Liu, M.H. Yu, W.L. Zhou, Appl. Phys. Lett. **87**, 172 505/1 (2005)
43 J. Cui, U.J. Gibson, J. Phys. Chem. B **109**, 22 074 (2005)
44 K.R. Kittilstved, W.K. Liu, D.R. Gamelin, Nat. Mater. **5**, 291 (2006)
45 Y.-H. Lee, J.-M. Yoo, D.-H. Park, D.H. Kim, B.K. Ju, Appl. Phys. Lett. **86**, 033 110 (2005)
46 A.B. Greytak, L.J. Lauhon, M.S. Gudiksen, C.M. Lieber, Appl. Phys. Lett. **84**, 4176 (2004)
47 S. Han, D. Zhang, C. Zhou, Appl. Phys. Lett. **88**, 133 109 (2006)
48 F.L. Deepak, P.V. Vanitha, A. Govindaraj, C.N.R. Rao, Chem. Phys. Lett. **374**, 314 (2003)
49 H.-J. Choi, H.-K. Seong, J. Chang, K.-I. Lee, Y.-J. Park, J.-J. Kim, S.-K. Lee, R. He, T. Kuykendall, P. Yang, Adv. Mater. **17**, 1351 (2005)
50 D.S. Han, J. Park, K.W. Rhie, S. Kim, J. Chang, Appl. Phys. Lett. **86**, 032 506/1 (2005)
51 Y. Shon, Y.H. Kwon, T.W. Kang, X. Fan, D. Fu, Y. Kim, J. Cryst. Growth **245**, 193 (2002)
52 K. Sardar, A.R. Raju, B. Bansal, V. Venkataraman, C.N.R. Rao, Solid State Commun. **125**, 55 (2003)
53 Y.D. Park, J.D. Lim, K.S. Suh, S.B. Shim, J.S. Lee, C.R. Abernathy, S.J. Pearton, Y.S. Kim, Z.G. Khim, R.G. Wilson, Phys. Rev. B **68**, 085 210/1 (2003)
54 J. Kim, F. Ren, G.T. Thaler, R. Frazier, C.R. Abernathy, S.J. Pearton, J.M. Zavada, R.G. Wilson, Appl. Phys. Lett. **82**, 1565 (2003)
55 D.S. Han, S.Y. Bae, H.W. Seo, Y.J. Kang, J. Park, G. Lee, J.-P. Ahn, S. Kim, J. Chang, J. Phys. Chem. B **109**, 9311 (2005)
56 N. Theodoropoulou, A.F. Hebard, M.E. Overberg, C.R. Abernathy, S.J. Pearton, S.N.G. Chu, R.G. Wilson, Phys. Rev. Lett. **89**, 107 203 (2002)
57 Y.M. Ksendzov, V.V. Makarov, Fiz. Tverd. Tela **12**, 3166 (1970)
58 J.S. Kulkarni, O. Kazakova, D. Erts, M.A. Morris, M.T. Shaw, J.D. Holmes, Chem. Mater. **17**, 3615 (2005)
59 O. Kazakova, J.S. Kulkarni, J.D. Holmes, S.O. Demokritov, Phys. Rev. B **72**, 094 415/1 (2005)
60 D. Erts, B. Polyakov, B. Daly, M.A. Morris, S. Ellingboe, J. Boland, J.D. Holmes, J. Phys. Chem. B **110**, 820 (2006)
61 K.J. Ziegler, B. Polyakov, J.S. Kulkarni, T.A. Crowley, K.M. Ryan, M.A. Morris, D. Erts, J.D. Holmes, J. Mater. Chem. **14**, 585 (2004)
62 F. D'Orazio, F. Lucari, N. Pinto, L. Morresi, R. Murri, J. Magn. Magn. Mater. **272–276**, 2006 (2004)
63 T. Dietl, Nat. Mater. **2**, 646 (2003)
64 H. Ohldag, V. Solinus, F.U. Hillebrecht, J.B. Goedkoop, M. Finazzi, F. Matsukura, H. Ohno, Appl. Phys. Lett. **76**, 2928 (2000)
65 J. Kudrnovsky, I. Turek, V. Drchal, F. Maca, P. Weinberger, P. Bruno, Phys. Rev. B **69**, 115 208/1 (2004)
66 T. Jungwirth, J. Masek, J. Sinova, A.H. MacDonald, Phys. Rev. B **68**, 161 202/1 (2003)
67 S.J. Pearton, C.R. Abernathy, G.T. Thaler, R. Frazier, F. Ren, A.F. Hebard, Y.D. Park, D.P. Norton, W. Tang, M. Stavola, J.M. Zavada, R.G. Wilson, Physica B **340–342**, 39 (2003)
68 X. Luo, S.B. Zhang, S.-H. Wei, Phys. Rev. B **70**, 033 308/1 (2004)
69 A.R. Phani, V. Grossi, M. Passacantando, L. Ottaviano, S. Santucci, in *Tech. Proc. 2006 NSTI Nanotechnology Conf. Trade Show*, Boston, 2006, p. 141
70 V.V. Osipov, A.M. Bratkovsky, Phys. Rev. B **70**, 205 312/1 (2004)